Evaluation of γ-Re_θ and k_L Transition Models on Riblet-Induced Transition Delay

Abdul Ahad Narejo, and Ekachai Juntasaro*

Mechanical Engineering (Simulation and Design),
The Sirindhorn International Thai-German Graduate School of Engineering (TGGS),
King Mongkut's University of Technology North Bangkok, Bangkok, 10800, Thailand
* Corresponding Author: Email: ekachaij@kmutnb.ac.th, Tel: +66(0)898971657, Fax: +66(0)29132500 ext. 2922

Abstract

Riblets are well known for the drag reduction when they are properly scaled. The transition delay is a key mechanism to reduce the drag force. For the first time, two popular transition models, i.e. γ-Re_θ and k_L models, are evaluated in this paper to simulate the flow over a combination of smooth and riblet surfaces. It is aimed to assess how realistically these two transition models can predict the transition delay induced by riblets. The LES data of Klumpp et al [3] are used for both the flow-condition calibration and the model evaluation in case of K-type transition and oblique transition. For flow over a totally smooth surface, the inlet flow condition is tuned up to match the RANS result with the LES data for each model. Under the same calibration, the response of both models to the riblets can be investigated when the fluid has to flow over a combination of smooth and riblet surfaces. It is found that the k_L model is more accurate for K-type transition while the γ-Re_θ model is more accurate for oblique transition. Moreover, the γ-Re_θ model has a better convergence rate for both types of transition.

Keywords*:* Laminar kinetic energy; Intermittency; Transition; Riblet; RANS.

1. Introduction

The riblet surface has been studied over the years for industrial applications. The researchers have attempted to design the optimal riblet surface that can reduce the utmost drag by delaying the transition. Wang et al. [8] used the laser doppler velocimeter (LDV) and hydrogen bubble flow visualization techniques to study the turbulent boundary layer flow over the riblet surface. The LDV system of high resolution can measure the velocity distribution in the viscous sublayer. It was found that the thickness of the viscous sublayer increased about 10% for the riblet surface compared to the smooth surface. They reported that the increase in the viscous sublayer thickness caused the buffer and log-law regions to move upward and the flow velocity increased, compared to the smooth surface case, and hence caused the drag reduction. The constant C in the log law was higher for the riblet surface compared to the smooth surface. That was the reason why the riblet surface possessed a lower friction velocity. It was also concluded

that the riblet surface had a little effect on flatness and skewness factors.

Lee and Lee [6] investigated the turbulent boundary layer over the riblets with semicircular grooves using the synchronized smoke wire method. The free-stream velocity was fixed at 3 m/s and 5 m/s, corresponding to drag decreasing (s^+=25.2) and drag increasing (s^+=40.6) conditions respectively, where the spacing of grooves s^+ is defined as $s^+=su_\tau/\nu$. In case of drag decreasing, the large scale longitudinal vortices were larger than the riblet spacing and most streamwise vortices stayed above the riblets and the flow inside the riblet valley remained calm. In case of drag increasing, the longitudinal vortices were smaller in size than the riblet spacing and most streamwise vortices stayed inside the riblet valley. Inside the riblet valley, the streamwise vortices interacted actively and hence increased the skin friction.

Lee and Jang [5] conducted the experiment using the particle image velocimetry (PIV) and smoke wire methods to control the flow around a NACA 0012 airfoil with a micro-riblet film. Two cases were investigated carefully: (i) airfoil grooved with a V-shaped micro-riblet film (MRF) and (ii) airfoil covered with a smooth polydimethylsiloxane (PDMS). Results were compared between the smooth film and the V-shaped MRF with the same thickness. The drag force on the MRF airfoil was about 6.6% lower than that on the smooth airfoil. The Reynolds shear stress and turbulent kinetic energy of both airfoils were almost similar or slightly higher in case of the MRF airfoil.

Litvinenko et al. [7] carried out the experiment on the influence of riblets on the development of a Λ-structure and its transformation into a turbulent spot. It was found that riblets prevented the transformation of the Λ-structure into the turbulent spot and that prevention led to a decay of this perturbation and the intensity of the Λ-structure on riblets, i.e. initially increased and then decayed to less than half of the level observed in case of the perturbation development on the smooth surface. It was concluded that the Λ-structure was stretched downstream on the smooth surface and transformed into the hairpin vortex whereas for a combination of smooth and riblet surfaces, the single Λ-structure and the turbulent spot generated oblique waves at the periphery.

Peet et al. [1] used LES with three customized Smagorinsky models to numerically simulate and investigate the turbulent drag reduction over straight and sinusoidal riblets. The results were compared with the DNS data of Choi et al. [9]. It was stated that the classical Smagorinsky model gave the best results. It was found that the wave length of the sinusoidal riblet was a crucial factor. It was also reported that the spanwise sinusoidal riblet could be an effective method for drag reduction compared to the conventional straight riblet because its drag reduction was almost 50% higher than the straight case. Finally, the reduction of crossflow turbulence intensity was responsible for the reduction of the turbulent effect on the skin friction drag.

Klumpp et al. [3,4] used LES to investigate the riblet controlled spatial transition in a zero pressure gradient boundary layer. They compared the skin friction coefficients of smooth and riblet surfaces for K-type transition and

oblique transition. They visualized the different stages of transition, that is, the two-dimensional TS waves which later deformed into the Λ-structure and then into hairpin vortices and finally into turbulence. The K-type transition and the oblique transition were discussed. In case of K-type transition, the development of three-dimensional Λ-vertex structures was slightly weakened by the riblets but no delayed breakdown of these structures into turbulence could be observed. In case of oblique transition, the breakdown to turbulence was delayed downstream since Λ-vortices and streamwisely aligned streaks were damped by the riblets. Finally it was reported that the riblets amplified two-dimensional TS waves and improved the drag reduction if properly distributed; otherwise could produce adverse effects. They found that when Λ-vortices occurred, the K-type transition took place as well. The Λ-structures deformed into streamwisely aligned vortices followed by turbulent breakdown. It was shown that the drag reduction could be achieved from 30% to 77% at different locations by delaying the turbulent state. It was also observed that there were vortices with a diameter equal to the riblet spacing.

2. Simulation Model

2.1 Domain Geometry

The same riblet geometry is used as in Klumpp et al. [3] to construct a combination of smooth and riblet surfaces. Table 1 summarizes the domain dimension of smooth and riblet surfaces and also the number of cells used.

Fig. 1 Riblet profile

The profile of the riblet surface is shown in Fig. 1., where $h_r/s=0.3$ and $b/s=0.1$ is used. The computational domain starts at the leading edge where $x/\delta_i \approx -209$. The Reynolds number $Re_{\delta,i}=U_\infty \delta_i/\nu$ based on the free-stream velocity and the displacement thickness is $Re_{\delta,i}=618$ at $x/\delta_i=0$ and the riblet structure begins at $x/\delta_i \approx 47$ according to Klumpp et al. [3]. The riblet surface requires finer mesh than the smooth surface due to the complex geometry and also to capture the transition (K-type transition and oblique transition) flow regime. To capture the transitional effects, $\Delta y^+ \leq 1$ is maintained for the first node above the wall. The FLUENT's built-in boundary adoption functions to improve y^+ are used.

2.2. Governing Equations

In this work, the steady three-dimensional incompressible flow is considered. The RANS transition models employed here can be summarized as follows:

2.2.1 Walters (k_L) Model

The Walters (k_L) model is based on three-equation eddy-viscosity model, which consists of the transport equations for the turbulent kinetic energy (k_T), the laminar kinetic energy (k_L) and the specific dissipation rate (ω) as follows:

$$\frac{\partial(\rho U_j k_T)}{\partial x_j} = P_{k_T} + R + R_{NAT} - \omega k_T - D_T + \frac{\partial}{\partial x_j}\left[\left(\nu + \frac{\alpha_T}{\alpha_k}\right)\frac{\partial k_T}{\partial x_j}\right] \quad (1)$$

$$\frac{\partial(\rho U_j k_L)}{\partial x_j} = P_{k_L} - R - R_{NAT} - D_L + \frac{\partial}{\partial x_j}\left[\nu \frac{\partial k_L}{\partial x_j}\right] \quad (2)$$

$$\frac{\partial(\rho U_j \omega)}{\partial x_j} = C_{\omega 1}\frac{\omega}{k_T}P_{k_T} + \left(\frac{C_{\omega R}}{f_W} - 1\right)\frac{\omega}{k_T}(R + R_{NAT}) - C_{\omega 2}\omega^2 + C_{\omega 3} f_\omega \alpha_T f^2{}_W \frac{\sqrt{k_T}}{d^3} + \frac{\partial}{\partial x_j}\left[\left(\nu + \frac{\alpha_T}{\alpha_\omega}\right)\frac{\partial \omega}{\partial x_j}\right] \quad (3)$$

2.2.1 Menter (γ-Re_θ) Model

The Menter (γ-Re_θ) model is based on the transport equation for the intermittency (γ) and the transport equation for the transition

momentum thickness Reynolds number $\overline{\mathrm{Re}_{\Theta t}}$ as follows:

$$\frac{\partial(\rho U_j \gamma)}{\partial x_j} = P_{\gamma 1} - E_{\gamma 1} + P_{\gamma 2} - E_{\gamma 2} + \frac{\partial}{\partial x_j}\left[\left(\mu + \frac{\mu_t}{\sigma_\gamma}\right)\frac{\partial \gamma}{\partial x_j}\right] \quad (4)$$

$$\frac{\partial(\rho U_j \overline{\mathrm{Re}_{\Theta t}})}{\partial x_j} = P_{\Theta t} + \frac{\partial}{\partial x_j}\left[\sigma_{\Theta t}(\mu + \mu_t)\frac{\partial \overline{\mathrm{Re}_{\Theta t}}}{\partial x_j}\right] \quad (5)$$

The detailed mathematical overview on Walters (k_L) and Menter (γ-Re_θ) models can be investigated in Ansys Fluent Theory Guide, Ansys, Inc. [1].

2.3. Boundary Conditions

Both built-in transition models in FLUENT version 12.1, i.e. Walters (k_L) and Menter (γ-Re_θ) models, are investigated by tuning up the inlet boundary conditions to approximately match the present results with the LES data of Klumpp et al. [3]. The inlet velocity of 8.9 *m/s* is used for all cases as used by Litvinenko et al [7]. Numerous simulations are carried out by varying (1) the viscosity ratio and free-stream turbulence intensity for K-type transition and (2) the spanwise velocity for oblique transition. The setup of the computational domain and boundary conditions is shown in Fig. 2. Parameters specified for boundary conditions are given in Tables 2 and 3 for Walters and Menter models respectively.

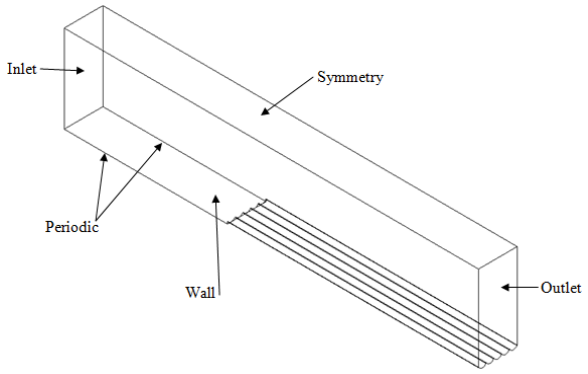

Fig. 2 Computational domain with boundary conditions

Table. 1 Domain dimensions.

Domain	L x W x H (mm)	Inlet (cells)	Outlet (cells)	Wall (cells)	Symmetry (cells)	Periodic (cells)	Domain (cells)
Smooth surface (K-type)	675x 6.05 x135	3120	3120	7800	7800	9000	138408
Riblet surface (K-type)	675x 6.05 x135	9120	9120	21408	4500	101750	6109675
Smooth surface (Oblique)	844x 6.05 x135	3120	3120	7800	7800	9000	138408
Riblet surface (Oblique)	844x 6.05 x135	9138	9120	27232	5620	127118	7632651

Table. 2 Boundary conditions for Walters model

Boundary condition	Smooth surface (K-type)	Riblet surface (K-type)	Smooth surface (Oblique)	Riblet surface (Oblique)
Inlet • Streamwise velocity • Spanwise velocity • Free-stream turbulence intensity • Viscosity ratio	 8.9 m/s 0 3% 700	 8.9 m/s 0 3% 700	 8.9 m/s 0.8 m/s 3% 700	 8.9 m/s 0.8 m/s 3% 700
Outlet	Zero pressure gradient	Zero pressure gradient	Zero pressure gradient	Zero pressure gradient
Wall	No slip	No slip	No slip	No slip
Periodic	Translational	Translational	Translational	Translational

Table. 3 Boundary conditions for Menter model

Boundary condition	Smooth surface (K-type)	Riblet surface (K-type)	Smooth surface (Oblique)	Riblet surface (Oblique)
Inlet • Streamwise velocity • Spanwise velocity • Free-stream turbulence intensity • Viscosity ratio	 8.9 m/s 0 2% 1500	 8.9 m/s 0 2% 1500	 8.9 m/s 0.08 m/s 2% 1500	 8.9 m/s 0.08 m/s 2% 1500
Outlet	Zero pressure gradient	Zero pressure gradient	Zero pressure gradient	Zero pressure gradient
Wall	No slip	No slip	No slip	No slip
Periodic	Translational	Translational	Translational	Translational

Table 4 Convergence rate using the residuals of 10^{-5}

Model	Smooth (K-type) (Number of iterations)	Riblet (K-type) (Number of iterations)	Smooth (Oblique) (Number of iterations)	Riblet (Oblique) (Number of iterations)
k_L	27960	2470	64000 (Not yet converged)	2090
γ-Re_θ	23600	865	1540	570

2.4. Computation Scheme

The pressure based solver using the finite volume method is employed for both models with default model constants, default solution methods and default solution controls. The convergence criteria of 10^{-5} are used for all simulation cases. The number of iterations is shown in Table 4 when the solution is converged,

except for the k_L model in case of the oblique transition on the smooth surface where the solution cannot be converged with this criterion.

3. Results and Discussion

In this section, the numerical results of K-type and oblique transition are presented and discussed to observe the difference between two transition models. The averaged C_f is plotted in all graphs.

3.1 K-type transition

Results for the smooth surface are shown in Fig. 3. Both models predict the fully turbulent regime slightly later as compared with the LES data. The reason is because the onset of transition is considered as the most important parameter during the calibration process to find the proper inlet boundary conditions. After running numerous simulations with various data sets of the viscosity ratio and free-stream turbulence intensity, it is observed that both models contaminate the C_f in the laminar regime. To investigate the contamination of C_f, the laminar model in FLUENT is selected and used with the same mesh resolution. The laminar solution is identical to the theoretical value as shown in Fig. 4.

Results for the riblet surface are shown in Fig. 5. The Walters model predicts C_f more accurately than the Menter model, especially the onset of transition and turbulence. Both models cannot predict C_f well in the region, where the riblet begins in the laminar regime, i.e. $x/\delta_i \approx 47$, and the Menter model predicts the fully turbulence regime quite late.

3.2 Oblique transition

Oblique transition is carried out by introducing a small velocity magnitude in the spanwise direction. Results for the smooth surface are shown in Fig. 6. Results show that both models predict an early transition onset. The Walters model predicts the turbulence onset early too while the Menter model shows the delay of the fully turbulence regime. However, the Menter model can predict the fully turbulence regime better than the Walters model. From results, both models cannot cope with oblique transition very well.

Results for the riblet surface are shown in Fig. 7. In this case, both models fail to predict the transition onset as well as the laminar regime when compared with the LES data. To some extent, the Menter model gives the slightly better fully turbulence regime than the Walters model. Both models predict higher C_f. However, both models can feel the transition delay due to the riblet, that is, the delay from $x/\delta_i \approx 200$ to $x/\delta_i \approx 300$ as predicted by both models compared to the delay from $x/\delta_i \approx 300$ to $x/\delta_i \approx 400$ in the LES data.

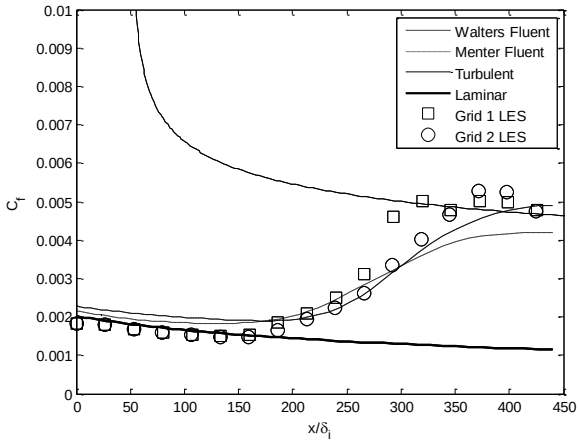

Fig. 3 Comparison of C_f in case of smooth surface K-type transition

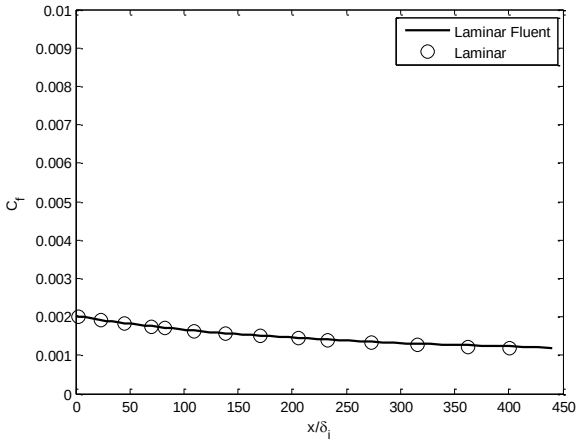

Fig. 4 Comparison of C_f in case of laminar flow

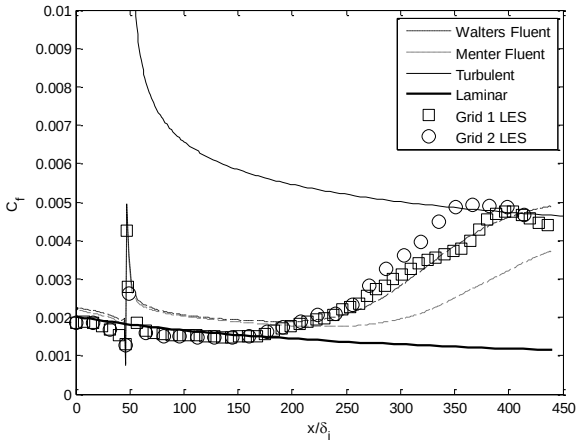

Fig. 5 Comparison of C_f in case of riblet K-type transition

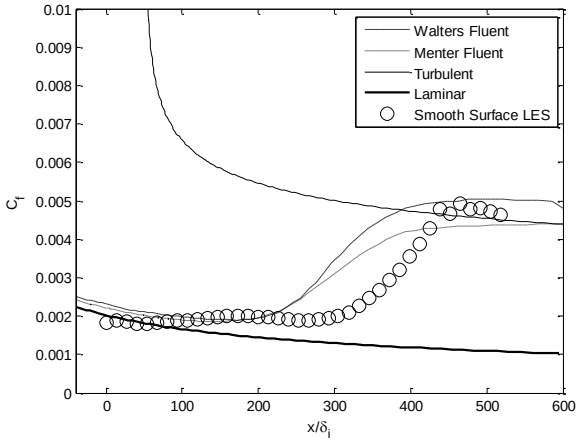

Fig. 6 Comparison of C_f in case of smooth surface oblique transition

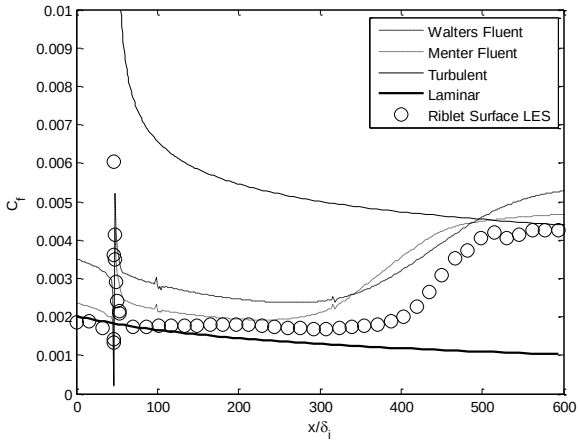

Fig. 7 Comparison of C_f in case of riblet oblique transition

4. Conclusion

All simulations are carried out in FLUENT version 12.1. Both models are calibrated on a totally smooth surface using different inlet flow conditions to match the same LES data. In case of K-type transition over a combination of smooth and riblet surfaces, it is found that the Walters model is closer to the LES data than the Menter model but the Menter model converges faster than the Walters model. In case of oblique transition over a combination of smooth and riblet surfaces, the Menter model is more accurate than the Walters model when compared to the LES data and the Menter model converges faster.

5. Acknowledgement

This research work is financially supported by the National Metal and Materials Technology Center (MTEC) under the grant number MT-B-52-MAC-21-198-G, which is greatly appreciated. Special thanks to Dr.-Ing Stephan Klumpp & Dr.-Ing Matthias Meinke at RWTH Aachen University, Aachen, Germany and Associate Professor Dr. Varangrat Juntasaro at Kasetsart University, Bangkok, Thailand for their technical contribution and discussion.

6. References

6.1 Articles in Journals

[1] Grek, G.R., Kozlov, V.V., Katasonov, M.M. and Chernorai. V.G. (2000). Experimental Study of a Λ-Structure Development and its Transformation into the Turbulent Spot, *Current Science*, vol. 79, No. 6, 25 pp. 781-789.

[2] Grek, G.R., Kozlov, V.V. and Titarenko, S.V. (1996). An Experimental Study of the Influence of Riblets on Transition, *J. Fluid Mech.,* vol. 315, pp. 31-49.

[3] Klumpp, S., Meinke, M. and Schröder, W. (2010). Numerical Simulations of Riblet Controlled Spatial Transition in a Zero Pressure-Gradient Boundary Layer, *Flow, Turbulence and Combustion*, vol. 85, No.1, pp. 57-71.

[4] Klumpp, S., Meinke, M. and Schröder, W. (2010). Numerical Simulations of Riblet Controlled Oblique Transition, *Seventh IUTAM Symposium on Laminar-Turbulent Transition*, IUTAM Bookseries, vol. 18, Part 2, pp. 207-212.

[5] Lee, S.J. and Jang, Y.-G. (2005). Control of Flow around a NACA 0012 Airfoil with a Micro- Riblet Film, *Journal of Fluids and Structures,* vol. 20, pp. 659-672.

[6] Lee, S.J. and Lee, S.-H. (2001). Flow Field Analysis of a Turbulent Boundary Layer over a Riblet Surface, *Experiments in Fluids,* vol. 30, pp. 153-166.

[7] Litvinenko, Y.A., Chernoray, V.G., Kozlov, V.V., Loefdahl, L., Grek, G.R. and Chun, H.H. (2006). The Influence of Riblets on the Development of a Λ Structure and its Transformation into a Turbulent Spot, *Doklady Physics*, vol. 51, No. 3, pp. 144–147.

[8] Wang, J.J., Lan, S.L. and Chen, G. (2000). Experimental Study on the Turbulent Boundary Layer Flow over Riblets Surface, *Fluid Dynamics Research*, vol. 27, pp. 217-229.

[9] Choi, H., Moin, P. and Kim, J. (1993). Direct Numerical Simulation of Turbulent Flow over Riblets, *J. Fluid Mech*., vol. 255, pp. 503-539.

6.2 Proceedings

[1] Peet, Y. and Sagaut, P. (2008). Turbulent Drag Reduction using Sinusoidal Riblets with Triangular Cross-Section, *38th AIAA Fluid Dynamics Conference and Exhibit*, 23-26 June 2008, Seattle, WA, USA.

[2] Zhang, H.Y., Yang, H.X. and Li, G. (2008). Numerical Study of Turbulent Drag Reduction over Riblet Surface, *Proceedings of the Eighteenth (2008) International Offshore and Polar Engineering Conference*, 6-11 July 2008, Vancouver, BC, Canada.

6.3 Books

[1] Ansys, Inc. (2009). Ansys Fluent 12.0 Theory Guide.